Functional Materials 17, No.3 (2010) 

# Ageing-dependent properties of ZnPc/C60 photovoltaic devices

*V.Kazukauskas, A.Arlauskas, M.Pranaitis, R.Lessmann*[*], *M.Riede*[*], *K.Leo*[*]

Semiconductor Physics Department and Institute of Applied Research of Vilnius University, Sauletekio al. 9, bldg. 3, LT-10222 Vilnius, Lithuania
[*]Institut fur Angewandte Photophysik, Technische Universitat Dresden, Dresden, Germany

*Received November 7, 2009*

The ZnPc/C60 solar cells with a reasonable energy conversion efficiency of ~1.5 % were investigated. The samples were aged for 1269 hours upon illumination by the blue LED with peak emission at 475 nm. Upon ageing, the devices have shown a strong and fast degradation of the efficiency, short circuit current and of the fill factor within several hours followed by a much slower decrease thereof. The carrier mobility dependences on electric field strength at different temperatures were measured by the Charge Extraction by Linearly Increasing Voltage method. The observed drop of device current cannot be explained be only mobility decrease. The increase of the effective barrier height by about 0.1 eV from ~0.55 eV up to ~0.65 eV was observed in the aged samples. Meanwhile, thermal activation energy values of the electrical conductivity grew from about 0.28 eV prior to degradation up to about 0.34 eV after ageing.

Исследованы солнечные элементы ZnPc/C60 с удовлетворительной эффективностью преобразования энергии (~1,5 %). Образцы были подвергнуты старению в течение 1629 ч путем облучения светом синего светодиода с длиной волны максимума излучения 475 нм. В процессе старения образцов обнаружено быстрое и значительное ухудшение эффективности, тока короткого замыкания и коэффициента заполнения в течение нескольких часов с последующим гораздо более медленным уменьшением этих параметров. Методом экстракции заряда линейно возрастающим напряжением измерены зависимости подвижности носителей от напряженности электрического поля при различных температурах. Наблюдаемое падение тока устройства не может быть объяснено только снижением подвижности. В состаренных образцах наблюдалось увеличение эффективной высоты барьера приблизительно на 0,1 эВ (от 0,55 до 0,65 эВ). Одновременно значения энергии термической активации электропроводности возрастали от приблизительно 0,28 эВ (перед старением) до приблизительно 0,34 эВ (после него).

## *1. Introduction*

Cu and Zn Phtalocyanines (CuPc and ZnPc), and C60 [1, 2] are materials often used in organic solar cell engineering. Their energy levels form a donor-acceptor junction, and they have high absorption coefficients and a complementary absorption for the Sun spectrum. C60 with its LUMO located at around 3.9 eV [3], is usually used as electron acceptor; it has a relatively high electron mobility up to ~1 $cm^2/Vs$ (neat layer, [4]). The heterojunction formed between C60 and CuPc or ZnPc can separate excitons formed in both materials. The HOMO of ZnPc is located around 5.1 eV. This kind of solar cells can supply the open circuit voltage ($V_{OC}$) of ~0.5–0.6 V, the short-circuit current density ($I_{SC}$) of about 10 $mA/cm^2$ and the fill factor (FF) of above 0.5–0.6, resulting in the energy conversion efficiency of about 3 %

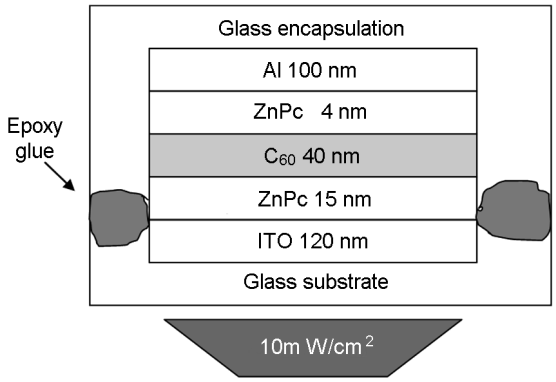


Fig. 1. Schematic representation of the sample cross section.

[5]. Other material combinations and/or tandem solar cells [6] yield even higher efficiencies reaching 5–6 % [7, 8]. However, the lifetime of high efficiency organic solar cells is still in the range of 1000 h, being too short for most real applications. This is mainly attributed to contamination with oxygen and moisture that can react with excited molecules. From the research of OLEDs, one can infer that in principle, organic molecules are very stable if not in contact with reactive species.

In this work, we have analysed the ageing and associated electrical properties (conductivity, the effective electron mobility, and energy parameters of material and interface) of the ZnPc devices.

We have analysed the device structures of ITO/ZnPc(15 nm)/C60(40 nm)/AOB (2 %) doped C60(4 nm)/Al(100 nm). The schematic layout of the sample cross section is presented in Fig. 1. Organic layers were deposited at a rate of 0.5 Å/s at a pressure below $5 \cdot 10^{-6}$ Pa, and Al was evaporated at 15 Å/s at a pressure below $10^{-4}$ Pa. The organic dopant was deposited at a rate of 0.02 Å/s. The thickness is measured with independent calibrated quartz crystal monitors. The devices were encapsulated. The encapsulation is done on the wafer with a glass cover that has a cavity with a getter inside.

The samples were aged for 1269 h at 35°C, illuminated by a blue LED, with incident light power density of 10 mW/cm$^2$ and peak emission at 475 nm, corresponding to an absorption peak of C60. The current-voltage (I-V) characteristics and their temperature and time dependences were measured upon ageing. The reference samples that were kept in dark at room temperature did show only very small changes in the I-V curves.

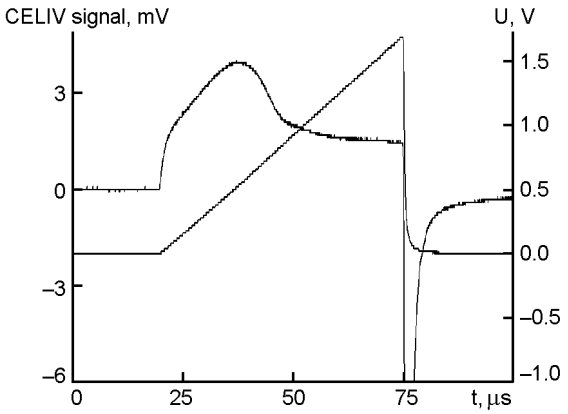


Fig. 2. Example of the CELIV plot demonstrating the characteristic maximum and the applied triangular voltage pulse.

## 2. Experimental

To measure the carrier mobility, the Charge Extraction by Linearly Increasing Voltage (CELIV) method was used [9]. In CELIV, a carrier extraction from the sample is assured by applying a triangular voltage pulse with a constant increase rate. The obtained CELIV plots, as e.g., presented in Fig. 2, demonstrate characteristic maxima, when the electric field in the sample becomes strong enough to extract most of the carriers. From these plots, the mobility can be calculated as

$$\mu = \frac{2d^2}{3At_{\max}^2\left[1 + 0.36\frac{\Delta j}{j(0)}\right]}, \quad (1)$$

and the sample conductivity can be found as

$$\sigma_0 = \frac{3\varepsilon\varepsilon_0\Delta j}{2t_{\max}j(0)}. \quad (2)$$

Here $A$ is the voltage increase rate; $t_{max}$, the time (measured from the pulse onset) when the characteristic maximum is observed; $d$, the sample thickness; $j(0)$, the plateau value corresponding to the capacitive displacement current of the sample; and $j$, the current spike height. In Eq. 1, the electric field redistribution effect during charge extraction is taken into account.

## 3. Results and discussion

*The cell parameters variation upon ageing.* The I-V curves obtained for one sample in dark and under illumination by the blue LEDs before and after the ageing are shown

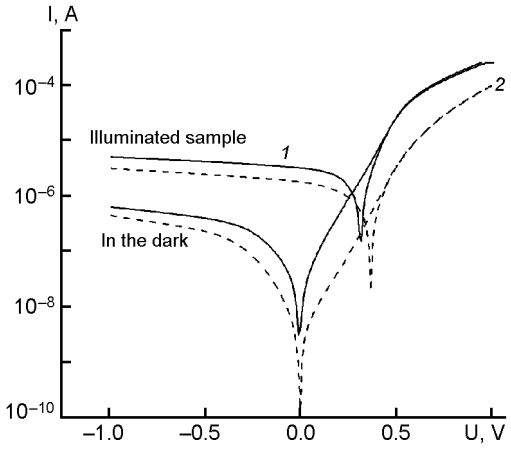


Fig. 3. IV curves in the dark and upon illumination by a blue LEDs prior to (curve *1*) and after the ageing (curve *2*).

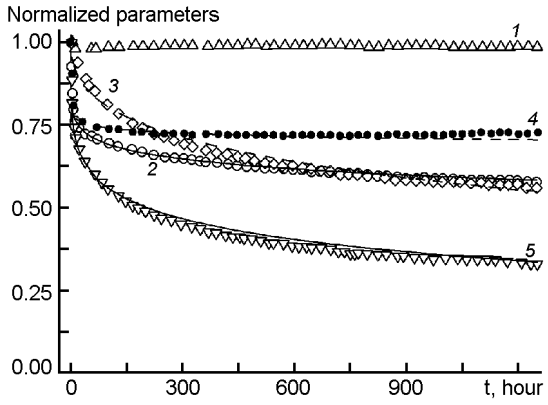


Fig. 4. Variation of the characteristic parameters for the investigated structure in time upon ageing (blue light, $T$ = 37°C). MP stands for the Maximum Power (MP). Points, experimental data; dashed curves, fittings by the stretched exponents.

in Fig. 3. In Table 1, the initial and final characteristic values after the ageing are presented. Fig. 4 shows the dynamics of the parameters of the illuminated sample upon ageing. A most prominent efficiency decrease occurs during first hours, and the decay is not a single exponential. The short circuit current ($I_{SC}$), the fill factor (FF) and the saturation ratio (defined as $I(-1V)/I_{SC}$) tend to stabilize after several hundred hours. The energy conversion efficiency degrades down to less than 50 % of the initial value, still tending to a final nonzero value. The degradation kinetics of all parameters except $V_{OC}$ could be described well by stretched exponents as, e.g., presented by Eqs. 3, 4 for $I_{SC}$ with different parameters:

$$I_{SC} = I_{SC}(t = 0)\ \exp\left[\left(-\frac{t}{\tau}\right)^{\beta}\right], \qquad (3)$$

$$t_{1/2} = \tau(\ln 2)^{1/\beta}. \qquad (4)$$

Here, $\tau$ and $\beta$ are parameters characterizing the stretched exponent, and $t_{1/2}$ is the half-lifetime of the relaxation. The time constants $\tau$ for the different cell parameters ranged from less than 900 h up to more than 10000 h. For most of the devices, $V_{OC}$ used to increase slightly or did not change. This behavior coincides with that of the potential barrier height described below.

*Thermally activated conductivity and potential barriers.* We had measured I-V dependences at different temperatures, an example is presented in Fig. 5. To analyse the I-V characteristics, we evaluated the influence of several mechanisms that are usually accounted for in organic devices. The necessity of that approach is clearly evidenced by the fact that the relative increase of the reverse current in Fig. 5 exceeds that of the forward current in the same temperature region. In the forward direction, dependence of the current is nearly exponential up to the voltages of about 0.5 V, and then the current increase becomes less expressed. In reverse direction, the current increase is much less pronounced and tends to saturate. The exponential behavior of current $I(U)$ on applied voltage $U$ and its saturation in reverse direction can be described by the Schottky barrier model as in [10]. This general diode equation describes the I-V characteristics of both p-n junctions and Schottky diodes:

Table 1. Characteristic values of the investigated cell prior to and after the ageing

| Time (h) | $V_{OC}$ (V) | $I_{SC}$ (μA) | Fill Factor (FF) | $I(-1\ V)/I_{SC}$ | Maximum Power (MP) (mW/cm$^2$) |
|---|---|---|---|---|---|
| 0 | 0.47 | 232 | 0.402 | 1.29 | 0.069 |
| 1269 | 0.47 | 154 | 0.232 | 1.57 | 0.027 |

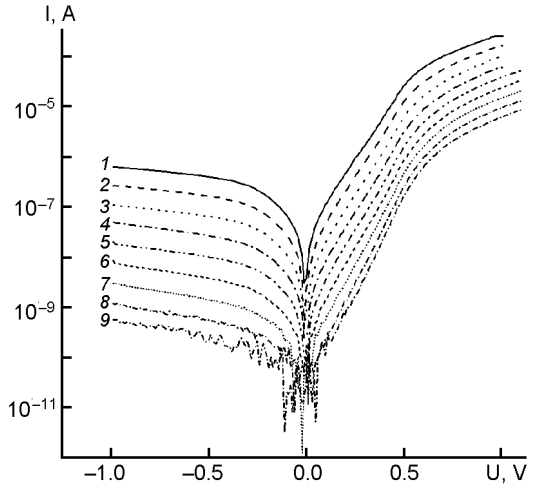


Fig. 5. IV curves of the reference sample measured in the dark at different temperatures: *1* – 310°C, *2* – 300°C, *3* –290°C, *4* – 280°C, *5* – 270°C, *6* – 260°C, *7* – 250°C, *8* – 240°C, *9* – 230°C.

$$I(U) = I_s\left[\exp\left(\frac{e(U - I(U)R_s)}{nkT}\right) - 1\right]. \quad (5)$$

Here, $I_s$ is the saturation current; $R_s$, the serial resistance of the sample volume; $n$, the ideality factor; $T$, temperature; $e$, the elementary charge; $k$, Boltzmann constant; $n = 1$ in the Shockley theory for $p$-$n$ junctions in the absence of recombination as well as for thermionic emission theory and diffusion theory for Schottky diodes. The ideality factor and the saturation current can be obtained from the slope and the intercept, respectively, obtained by extrapolation of the linear part of the semilogarithmic plot of $I$ vs $U$. The saturation current density is given by:

$$j_s = A^*\,T^2\exp\left(-\frac{e\Phi_B}{kT}\right). \quad (6)$$

Here, $A^*$ is the Richardson constant and $\Phi_B$ is a contact potential barrier. Therefore, using Eq. 6, the contact potential barrier height can be evaluated from the temperature dependence of the reverse current. The plots of the reverse and forward current values are presented in Fig. 6 for the reference sample and the aged ones. The characteristic contact barrier is seen to be about 0.55 eV in the reference sample, similar to other evaluations, e.g., [6, 11]. After degradation, it increases by about 0.08 eV (up to 0.63 eV). It is necessary to note that, as pointed above, $V_{OC}$, which is related with the potential barrier height, also increases

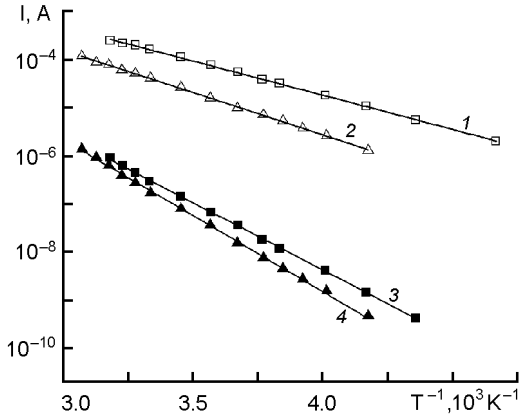


Fig. 6. Temperature dependences of the forward and reverse current values measured at –0.9 V (filled symbols) and +0.9 V (open symbols), respectively, for two samples: the reference (squares) and the aged one (triangles).

slightly in the aged samples. Therefore, this barrier difference can be supposed to increase due to degradation.

The slow growth of the reverse current with voltage could be due to the field-assisted thermionic injection over the image force barrier (Schottky effect) [12]:

$$j = AF^{3/4}\exp\left(2\sqrt{\frac{e\gamma}{kT}F}\right). \quad (7)$$

Here, $F$ is electric field; $\gamma = e^2/16\pi\varepsilon\varepsilon_0 kT$, and $A(F) = const$. Unfortunately this model, though explaining the field dependence of the reverse current, does not give any numerical values characterizing the barrier.

In the forward direction. The exponential growth prevails up to about 0.5–0.6 V, what coincides with the height of the contact potential barrier. Above that point, another current limiting mechanism starts playing a role. To analyse the temperature dependence of the forward current in this mode, one has to take into account also the exponential dependence of the sample volume resistance (due to either thermal generation of carriers or their mobility variation with temperature):

$$R_s = R_{s0}\exp\left(\frac{eE_A}{kT}\right). \quad (8)$$

Here, $E_A$ is the effective thermal activation energy of the sample resistance. Therefore, the lower activation energy values in forward direction evaluated from Fig. 6 characterize just the thermal activation energy values of the sample conductivity. Again, slightly lower values of about

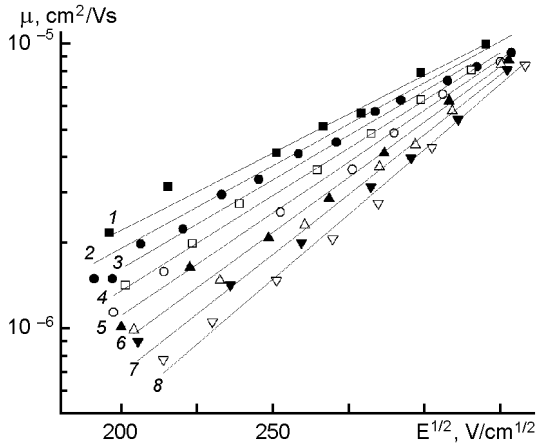


Fig. 7. Carrier mobility dependences on applied electric field strength at different temperatures: (*1* – 310°C, *2* – 300°C, *3* –290°C, *4* – 280°C, *5* – 270°C, *6* – 260°C, *7* – 250°C, *8* – 240°C) in the reference sample. Lines represent fitting of the data by the Gaussian

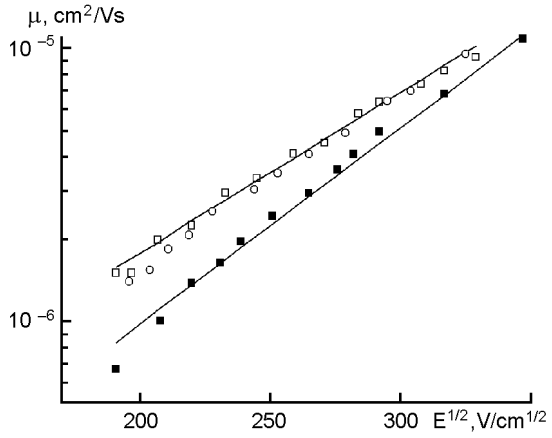


Fig. 8. Carrier mobility dependences on applied electric field strength at 300 K in the reference sample (open symbols) and the aged structure (filled squares). Lines represent fitting of the experimental data by the Gaussian Disorder Model according to Eq. 9.

0.28 eV are characteristic for the reference sample, and they grow up to about 0.34 eV after ageing.

We have fitted the experimental dependences presented in Fig. 5 by Eqs. 5–8 and a good agreement was achieved with the fitting parameters similar to above, the ideality factor $n$ approximating 3.1 and the sample resistance of about 1650Ω at 300 K. The ideality factor is relatively high, but in many cases in organic structures even the best reported values exceed 2–2.2 [10]. Moreover, it was found in [13] that $n$ in ZnPc devices linearly depends on reciprocal temperature.

*Charge carrier mobility*. The carrier mobility dependences in the reference sample on electric field strength at different temperatures are presented in Fig. 7. The comparison of mobility behavior at $T = 300$ K in both sample types is presented in Fig. 8. It is seen that in the investigated samples, the usual mobility increase with electric filed prevails, in contrast to the so-called negative mobility behavior that could be observed in highly spatially inhomogeneous materials [14, 15]. To analyse the mobility behavior, we have used the Gaussian Disorder Model (GDM). In the GDM, the charge transport in disordered organic conductors is supposed to proceed by means of hopping in a Gaussian site-energy distribution. This density of states (DOS) reflects the energy spread in the charge transporting levels of chain segments due to fluctuation in conjugation lengths and structural disorder. Within the Gaussian disorder model, the mobility is given by [16]:

$$\mu(F,T) = \mu_\infty \exp\left[-\left(\frac{2\sigma}{3kT^2}\right)^2\right] \exp\left\{C\left[\left(\frac{\sigma}{kT}\right)^2 - \Sigma^2\right]\sqrt{F}\right\}. \quad (9)$$

This equation was derived from Monte-Carlo simulations of the charge carrier hopping processes in a material with energy (σ) and positional disorder (Σ) described by Gaussian distribution functions. $\mu_\infty$ is the high temperature mobility limit and $C$ is a specific parameter that is obtained from the simulations as $C = 2.9 \cdot 10^{-4}$ $(\mathrm{cm/V})^{1/2}$. Therefore, the GDM was used to fit the experimental data as presented in Figs.7, 8 by solid lines. We have used the same fitting parameters for the single samples, only the temperature being varied. The fitting values obtained for the pristine and the aged samples are given in Table 2.

It can be seen that both energy and spatial disorder parameters increase considerably in the aged sample, similar to the energy parameters obtained from the I-V measurements. Therefore, the hopping carrier transport can be supposed to become aggravated upon ageing due to increasing of both energetic and spatial disorder of the hopping states. First of all, this results logically in decrease of the sample conductivity as well as growth of its activation energy. Indeed, to take part in conductivity, carriers have to move in a greater energy

Table 2. Fitting parameters of the GDM model used to fit mobility the behavior in the pristine and aged samples

| Parametres | Samples | |
|---|---|---|
| | Reference sample | Aged sample |
| $\Sigma$ | 0.2 | 0.7 |
| $\sigma$(eV) | 0.0955 | 0.107 |
| $\mu_\infty$(cm$^2$/Vs) | $5.00 \cdot 10^{-5}$ | $7.00 \cdot 10^{-5}$ |
| $C$ (cm/V)$^{0.5}$ | $1.00 \cdot 10^{-3}$ | $1.00 \cdot 10^{-3}$ |

and spatial disorder, meaning that their jumps between hopping states have to be more energized. Moreover, the increasing material disorder results also in the increase of the mean potential barrier height that governs the carrier flow over the barrier providing the rectifying behavior.

## *4. Summary and conclusions*

We have presented the ageing properties investigation of ZnPc/C60 solar cells as those are influenced by the variation of energy parameters characterizing material conductivity, potential barrier height, and charge carrier mobility. The simple test device structure shows a reasonable conversion efficiency of about 1.5 %.

The devices aged under illumination show a strong and fast degradation of the short circuit current and fill factor after several hours followed by an almost constant behavior of these values. The reference samples kept in the dark at the room temperature show only very small changes in the I-V curves. The parameters characterizing the potential barrier height providing the diode-like behavior and the activation energy value of material conductivity were evaluated from I-V dependences at different temperatures. It was found that the potential barrier of about 0.55 eV evaluated in the reference sample, increased after degradation up to 0.63 eV. Meanwhile, thermal activation energy of the electrical conductivity grows from about 0.28 eV prior to degradation up to about 0.34 eV after ageing.

Carrier mobility dependences on electric field strength at different temperatures were measured by the Charge Extraction by Linearly Increasing Voltage (CELIV) method. It was demonstrated that the mobility decreases during degradation as compared to the reference samples. These changes result from the increase of both energy ($\sigma$) and positional disorder ($\Sigma$) parameters within the Gaussian Disorder Model. Therefore, the hopping carrier transport becomes aggravated, resulting in decrease of the sample conductivity as well as in growth of its activation energy. This means that the jumps of the carriers between hopping states have to be energized more to move in a greater energetic and spatial disorder in order to take part in conductivity. Moreover, increasing material disorder also causes growth of the mean potential barrier height that governs carrier flow over the barrier providing the diode-like behaviour.

*Acknowledgements*. R.Lessmann acknowledges CAPES/Brazil and DAAD for the scholarship. A.Arlauskas acknowledges Student Research Fellowship Award from the Lithuanian Science Council. Part of this work was performed within the EC FP6 project OrgaPVNet.

## *References*

1. C.W.Tang, *Appl. Phys. Lett.*, **48**, 183 (1986).
2. T.Taima, S.Toyoshima, K.Hara et al., *Jap. J. Appl. Phys.*, Part 2, **45**, L217 (2006).
3. R.W.Lof, M.A.van Veenandaal et al., *Phys. Rev. Lett.*, **68**, 3924 (1992).
4. Th.B.Singh, N.Marjanovic, G.J.Matt et al., *Org. Electron.*, **6**, 105 (2005).
5. S.Pfuetzner, J.Meiss, A.Petrich et al., *Appl. Phys. Lett.*, **94**, 253303 (2009).
6. D.Gebeyehu, B.Maennig, J.Drechsel et al., *Sol. Energy Mater. Sol. Cells*, **79**, 81 (2003).
7. M.A.Green, K.Emery, Y.Hishikawa et al., *Prog. Photovolt:Res. Appl.*, **17**, 85 (2009).
8. J.Y.Kim, K.Lee, N.E.Coates et al., *Science*, **317**, 222 (2007).
9. G.Juska, K.Arlauskas, M.Viliunas et al., *Phys. Rev. Lett.*, **84**, 4946 (2000).
10. W.Riess, In: Organic Electroluminescent Materials and Devices, ed. by S.Miyata and H.S.Nalva, Gordon and Breach, Amsterdam (1997), p.73.
11. M.Egginger, R.Koeppe, F.Meghdadi et al., *Proc. SPIE*, **6192**, 348 (2006).
12. J.Godlewski, J.Kalinowski, *Jap. J. Appl. Phys.*, **28**, 24 (1989).
13. K.Harada, A.G.Werner, M.Pfeiffer et al., *Phys. Rev. Lett.*, **94**, 036601 (2005).
14. A.J.Mozer, N.S.Sariciftci, A.Pivrikas et al., *Phys. Rev. B*, **71**, 035214 (2005).
15. V.Kazukauskas, M.Pranaitis, L.Sicot et al., *Mol. Cryst. Liq. Cryst.*, **447**, 459 (2006).
16. H.Baessler, *Phys. Stat. Solidi(b)*, **175**, 15 (1993).

# Залежність властивостей фотогальванічних елементів ZnPc/C60 від старіння

***В.Кажукаускас, А.Арлаускас, М.Пранайтіс, Р.Лессманн, М.Ріде, К.Лео***

Досліджено сонячні елементи ZnPc/C60 з задовільною ефективністю перетворення енергії ~1,5 %. Зразки піддано старінню протягом 1629 год шляхом опромінення світлом синього світлодіода з довжиною хвилі у максимумі випромінювання 475 нм. У процесі старіння зразків виявлено швидке та значне погіршення ефективності струму короткого замикання та коефіцієнта заповнення протягом кількох годин з наступним значно повільнішим зменшенням цих параметрів. Методом зняття заряду лінійно зростаючою напругою виміряно залежності рухомості носіїв від напруженості електричного поля при різних температурах. Виявлене спадання струму елемента не може бути пояснено тільки зниженням рухомості. У зразках після старіння спостерігалося збільшення ефективної висоти бар'єру приблизно на 0,1 еВ (від 0,55 до 0,65 еВ). Одночасно значення енергії термічної активації електропровідності зростали від приблизно 0,28 еВ (перед старінням) до приблизно 0,34 еВ (після нього).